

System-Wide Effects of Local Bed Disturbance on the Morphological Evolution of a Bifurcating Channel Network

Gao, Weilun; Shao, Dongdong; Wang, Zheng Bing; Zhu, Zhenchang; Yang, Zhifeng

DOI

[10.1029/2023JF007514](https://doi.org/10.1029/2023JF007514)

Publication date

2024

Document Version

Final published version

Published in

Journal of Geophysical Research: Earth Surface

Citation (APA)

Gao, W., Shao, D., Wang, Z. B., Zhu, Z., & Yang, Z. (2024). System-Wide Effects of Local Bed Disturbance on the Morphological Evolution of a Bifurcating Channel Network. *Journal of Geophysical Research: Earth Surface*, 129(3), Article e2023JF007514. <https://doi.org/10.1029/2023JF007514>

Important note

To cite this publication, please use the final published version (if applicable). Please check the document version above.

Copyright

Other than for strictly personal use, it is not permitted to download, forward or distribute the text or part of it, without the consent of the author(s) and/or copyright holder(s), unless the work is under an open content license such as Creative Commons.

Takedown policy

Please contact us and provide details if you believe this document breaches copyrights. We will remove access to the work immediately and investigate your claim.

Green Open Access added to TU Delft Institutional Repository

'You share, we take care!' - Taverne project

<https://www.openaccess.nl/en/you-share-we-take-care>

Otherwise as indicated in the copyright section: the publisher is the copyright holder of this work and the author uses the Dutch legislation to make this work public.

JGR Earth Surface

RESEARCH ARTICLE

10.1029/2023JF007514

Special Section:

Prediction in coastal geomorphology

Key Points:

- Local deepening in one branch can lead to a system-wide morphological response of the bifurcating channel network in a two-stage pattern
- The system-wide effects arise from the altered water surface slope downstream of the bifurcation due to the local deepening
- The recovery of the equilibrium configuration of a bifurcating channel network is much longer than that of a comparable single channel

Supporting Information:

Supporting Information may be found in the online version of this article.

Correspondence to:

D. Shao and Z. Yang,
ddshao@bnu.edu.cn;
zfyang@gdut.edu.cn




Citation:

Gao, W., Shao, D., Wang, Z. B., Zhu, Z., & Yang, Z. (2024). System-wide effects of local bed disturbance on the morphological evolution of a bifurcating channel network. *Journal of Geophysical Research: Earth Surface*, 129, e2023JF007514. <https://doi.org/10.1029/2023JF007514>

Received 8 NOV 2023

Accepted 13 FEB 2024

System-Wide Effects of Local Bed Disturbance on the Morphological Evolution of a Bifurcating Channel Network

Weilun Gao¹ , Dongdong Shao² , Zheng Bing Wang^{3,4} , Zhenchang Zhu^{1,5}, and Zhifeng Yang^{1,5}

¹Guangdong Provincial Key Laboratory of Water Quality Improvement and Ecological Restoration for Watersheds, School of Ecology, Environment and Resources, Guangdong University of Technology, Guangzhou, China, ²State Key Laboratory of Water Environment Simulation, School of Environment, Beijing Normal University, Beijing, China, ³Faculty of Civil Engineering and Geosciences, Delft University of Technology, Delft, The Netherlands, ⁴Deltares, Delft, The Netherlands, ⁵Southern Marine Science and Engineering Guangdong Laboratory (Guangzhou), Guangzhou, China

Abstract Deltaic channel networks are important conduits for water and material supplies to the fluvial and coastal communities. However, increasing human interventions in river deltas have altered the topology and geometry of channel networks as well as their long-term evolution. While the morphological evolution of a single channel has received extensive studies, the system-wide morphological responses of channel networks to local disturbances remain largely unclear. Here we investigate the morphological responses of a bifurcating channel network subject to local disturbance of channel deepening due to dredging and sand mining through idealized simulations, and further compare the results with the reference scenarios of a single channel and theoretical analysis of the phase plane. The results show that the infilling of the local deepening is associated with the erosion of the entire branch, which also causes system-wide effects on the siltation of the other branch. The morphological responses of the bifurcating channel network consist of a relatively short stage for the infilling of the local deepening followed by a relatively long stage for recovering the equilibrium configuration of the river bifurcation. The system-wide effects of the local disturbance arise from the altered water surface slope and water partitioning downstream of the bifurcation due to the local deepening. Also, the prolonged recovery of the equilibrium configuration is consistent with theoretical analysis, which reveals a slow evolution of the bifurcation when approaching the equilibrium. Our results can help understand the long-term morphological responses of large-scale complex channel networks and inform water managements under increasing human interventions.

Plain Language Summary River channel networks with multiple interconnected channels are common in river deltas and are critical for the transport of water, sediment and nutrients to riverine and coastal wetlands. Intensive human interventions, such as dredging and sand mining, can lead to local disturbance of bed deepening in the channel networks. However, the system-wide responses of the channel network to such local disturbances, for example, the morphological changes in neighboring channels as a result of a local deepening in one channel, remain elusive. In this study, we selected a bifurcating channel network, where the upstream river channel splits into two branches, as a simple demonstration case of a channel network to address this issue. We simulated the system-wide responses of the bifurcating channel network to local deepening in one of the branches through numerical experiments in the Delft3D model. The results showed that the local deepening in one branch can affect the entire channel network, such as the siltation of the other branch. Moreover, the system-wide effects on the channel network last much longer than a comparable single channel with the same total channel width and length. Our results can help inform the restoration and management of channel networks under increasing human interventions.

1. Introduction

Channel networks form in river deltas mainly due to the formation of river mouth bars, avulsions and levee breaches (Gao et al., 2018; Jerolmack, 2009; Ke et al., 2019; Konkol et al., 2022). The topology and channel geometry of channel networks play an important role in distributing water and materials (such as sediments, nutrients and larvae) in fluvial and coastal wetlands, which is critical for the sustainability of deltaic communities (Hoitink et al., 2020; Passalacqua & Moodie, 2022). Human activities, such as dredging, sand mining, reclamation, and embankment construction, have significantly altered the topology, bed level and channel width of deltaic channel networks (Cox et al., 2021; Luo et al., 2007; Shaw et al., 2021; van Maren et al., 2023). These

disturbances further affect the long-term morphological evolution of channel networks (Edmonds et al., 2010; Jeuken & Wang, 2010; Syvitski & Saito, 2007; van Maren et al., 2023). Therefore, it is critical to understand the morphological responses of channel networks to human interventions under ever-increasing environmental changes (Best, 2019; Hoitink et al., 2020; Passalacqua et al., 2021; Wang et al., 2015).

In engineered rivers where the network topology and channel widths are fixed, the responses of river channels to disturbances are limited to the adjustment of channel slope, water depth, and bed surface texture (Blom, Arkesteijn, et al., 2017; Chowdhury et al., 2023). In single-thread fluvial channels, their morphological evolution under disturbances has received extensive attention (Best, 2019; Wohl et al., 2015). With fixed channel width, the evolution of longitudinal profile of river channel under human interventions or natural changes has become the main focus (Blom, Arkesteijn, et al., 2017; Gao, Nienhuis, et al., 2020; Wang et al., 2008; Ylla Arbós et al., 2023; Zheng et al., 2022). This is basically built upon the in-depth understanding of the equilibrium longitudinal profiles of river channels thus far (Blom et al., 2016; Chang, 1986; Ferrer-Boix et al., 2016; Gao, Li, et al., 2020). The morphological evolution of the river channel always proceeds toward an equilibrium longitudinal profile (Jansen et al., 1979), that is, a combination of water depth and slope that can exactly transport the upstream supplied sediment to the downstream, as initially proposed by Mackin (1948). The question on the responses of river channels to disturbance lies in the predictions of the path to the equilibrium, such as the timescale for approaching the equilibrium and the spatial propagation of the disturbance (Blom, Chavarrías, et al., 2017; Doyle & Harbor, 2003; Wu et al., 2012).

In a complex channel network consisting of multiple bifurcations and several interconnected channels, the morphological responses of river channels to disturbances, such as changing river discharges, embankment construction and dredging activities, have also been explored (Chowdhury et al., 2023; Edmonds et al., 2010; van Maren et al., 2023). These studies have shown that local disturbance can lead to the morphological responses of each channel in the network, suggesting a system-wide response of the channel network to local disturbance. The system-wide response can be heterogeneous, that is, some channels can be silted and closed off while others can be eroded and expanded. Nonetheless, a close examination of the system-wide responses of complex channel networks to local disturbances is still elusive. This is largely due to the lack of understanding on equilibrium configurations of complex channel networks (Kleinhans et al., 2012; Salter et al., 2020).

In deltaic channel networks, river bifurcation is a common morphological feature that splits an upstream channel into two downstream branches, forming a simple yet basic bifurcating channel network with three interconnected channels (Figure 1) (Kleinhans et al., 2013). Several equilibrium configurations (the equilibrium water depths and slopes in each channel) have been recognized for the channel network of a single river bifurcation, indicating whether two branches remain open in an (a)symmetric configuration or one of the branches closes off (Bolla Pittaluga et al., 2003, 2015; Edmonds & Slingerland, 2008; Iwantoro et al., 2021; Redolfi et al., 2019; Slingerland & Smith, 1998; Wang et al., 1995). A symmetric equilibrium configuration indicates that the two branches have identical channel geometry and river discharges. An asymmetric equilibrium configuration indicates that one of the branches is deeper and conveys more river discharges (i.e., the dominant branch), and the other branch is shallower and conveys less river discharges (i.e., the subordinate branch). These findings have been applied to explain the evolution of river bifurcations under disturbances, such as changing river discharge, dredging, and chute cutoffs (Edmonds et al., 2010; Jeuken & Wang, 2010; van Dijk et al., 2014).

Previous studies have recognized the mutual interactions between different branches connected to the bifurcation (Ragno et al., 2022; Salter et al., 2018, 2020). Therefore, the morphological responses of channel networks to disturbances are highly intricate processes because the propagation of disturbance would change the water and sediment supplied to each channel via the hydrodynamic and morphodynamic adjustments of the river bifurcations (Chowdhury et al., 2023; Kleinhans et al., 2008). The changing water and sediment supplies would further affect the morphological evolution of each channel (Ragno et al., 2021; Salter et al., 2020). While extensive studies have focused on the mechanisms leading to different equilibrium configurations of river bifurcations (see the reviews in Kleinhans et al. (2013) and Edmonds et al. (2021)), the responses of equilibrium river bifurcations to disturbance, especially the propagation of the disturbance and its morphological timescale for recovering the equilibrium, have received limited attention.

In this study, we mainly focus on the local disturbance of the channel deepening caused by dredging or sand mining (hereinafter termed the “borrow-pit”) (Chen et al., 2010; Eslami et al., 2019; Jeuken & Wang, 2010; Luo et al., 2007; Yuill et al., 2016), since these activities are pervasive in the world's deltas, such as the

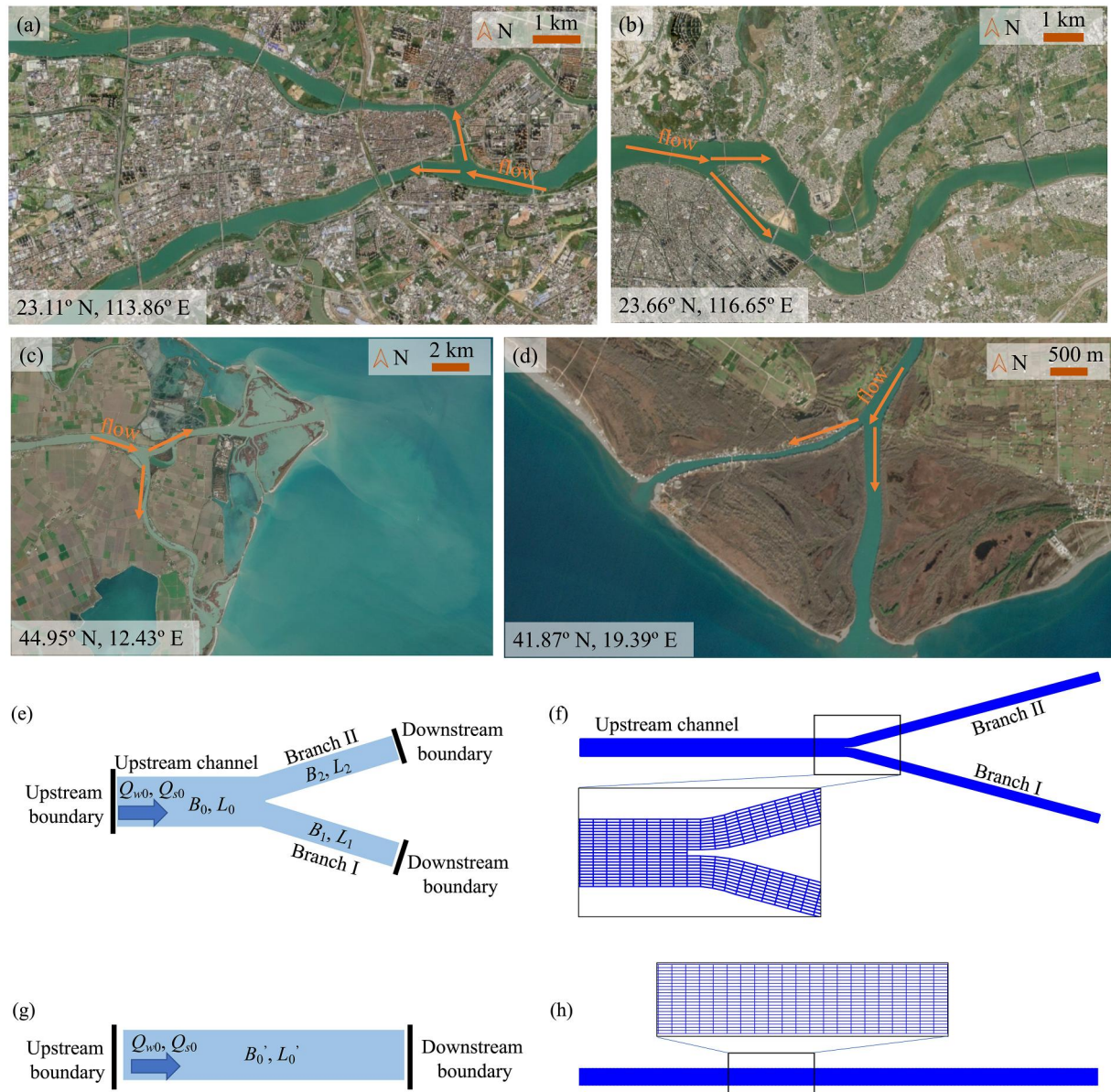


Figure 1. Examples of bifurcations in river deltas: (a) the Dongjiang Delta (a subdelta of the Pearl River Delta) and (b) the Hanjiang Delta, in Guangdong, China, (c) the Po River Delta, Italy, and (d) the Bojana River Delta, Montenegro. The schematization of (e) channel network of river bifurcation and (g) a single river channel as well as their computational domains (panels f, h). See the main text for the definitions of the variables. Satellite images are from the Copernicus Sentinel data (<https://dataspace.copernicus.eu/>).

Mississippi-Atchafalaya Delta (Shaw et al., 2021; Yuill et al., 2016), the Pearl River Delta and Yangtze River Estuary, China (Luo et al., 2007; Wang et al., 2015), the Mekong River Delta, Vietnam (Anthony et al., 2015), and the Rhine-Meuse Delta, the Netherlands (Cox et al., 2021). For example, the historical sand mining in the deltaic channels of the Pearl River Delta was up to $7 \times 10^7 \text{ m}^3/\text{yr}$ during the 1980s–2000s, which was unevenly distributed in the channel network and has led to the alterations in water partitioning at the bifurcations of the network (Luo et al., 2007). The dredging activities for navigation have been conducted between 1932 and 1950 in the lower reach of the Atchafalaya River, which accounted for 35% of the increased river discharge in the Atchafalaya River through the Mississippi-Atchafalaya bifurcation (Shaw et al., 2021). Understanding the responses of river bifurcations to local disturbances of dredging and sand mining can provide insights into the stability and resilience of channel networks and inform their protection and restoration under increasing human interventions (Cox et al., 2021; Shaw et al., 2021; Wang et al., 2015).

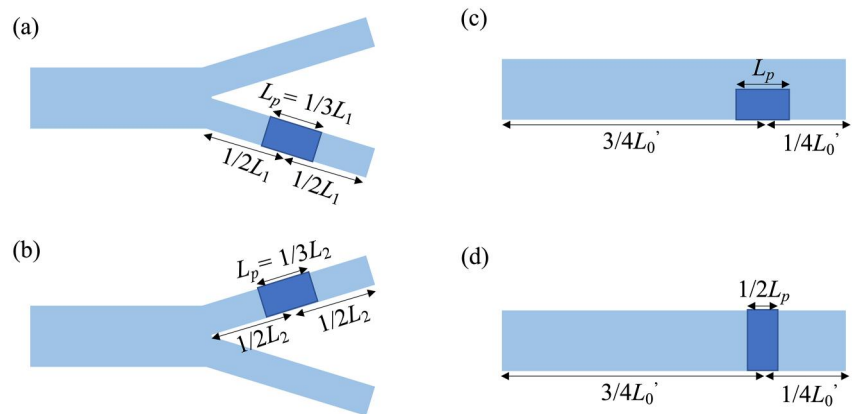


Figure 2. Different scenarios of local disturbance of channel deepening for the channel network (panels a, b) and the single channel (panels c, d). The dark blue area indicates the locations of the local deepening of the borrow-pits. L_p is the length of the borrow-pit, L_1 and L_2 are the lengths of the two branches ($L_1 = L_2$), and L_0' ($=2L_1$) is the length of the single channel.

In this study, we aim to investigate the spatial propagation of local disturbance of channel deepening in the bifurcating channel networks and the timescale for recovering the morphological equilibrium. Numerical simulations were conducted to explore the morphological evolution of the bifurcating channel networks under different scenarios of local disturbance of channel deepening due to dredging and sand mining. We focused on channel networks with a single bifurcation in river-dominated deltas where riverine forcing is the main focus. The effects of tides, waves and salinity on the morphological evolution of channel networks are negligible and thus not considered. The channel widths are fixed and the adjustments of the river channels of the networks are through channel depths and bed slopes. The results were compared with the reference scenarios of a single channel without bifurcation and theoretical analyses of the phase plane. Notably, we focus on the morphological evolution of the channel network (and the single channel) after the formation of an initial borrow-pit (Figure 2); therefore, we do not consider the periods during which the borrow-pit is created and the scenarios of continuous dredging.

2. Methodology

2.1. Model Setup

In this study, we simulated the morphological evolution of bifurcating channel networks under local disturbances using the Delft3D model. The results were further compared with those of a single river channel. We used idealized numerical simulations with schematized geometry and generic modeling parameters to investigate and quantify the relevant effects. The schematization of the channel networks as well as the single channels and their computational domains are provided in Figure 1. In this study, we used the two-dimensional depth-averaged version of the Delft3D model, which solves shallow water equations for the hydrodynamics (see Lesser et al. (2004) for more details). Hydrodynamics, sediment transport, and morphodynamics are online-coupled. Notably, since we focus on sand-bed channel networks, the sediment transport formula adopted in this study is Engelund and Hansen (1967)'s formula, which reads

$$Q_s = B\sqrt{Rgd_{50}^3}m(\theta)^n \quad (1)$$

where Q_s is the sediment transport capacity, R ($=1.65$) is the submerged specific density of sediment, g is gravitational acceleration, d_{50} is sediment grain size, $m = 0.05 C^2/g$ and $n = 2.5$ are empirical coefficients, B and θ are the channel width and Shields stress, respectively.

For the channel network of the river bifurcation (Figure 1e), the upstream channel width (B_0) and length (L_0) are 200 and 3,000 m, respectively. The upstream channel splits into two identical branches with halved width of the upstream channel (i.e., $B_1 = B_2 = 100$ m) and identical channel lengths $L_1 = L_2 = 3,000$ m. For the single river channel (Figure 1g), it has the same total channel width and length as the channel network, that is, the channel

Table 1

The Channel Geometry (B_0 , D_0 , and S_0), Boundary Conditions (Upstream River Discharge Q_{w0} and Sediment Load Q_{s0}) and Sediment Grain Size (d_{50}) That Lead to Different Shields Stress (θ_0) and Width-To-Depth Ratio (β_0) for the Numerical Scenarios in This Study

RunID	Shields stress θ_0	Width-to-depth ratio β_0	Channel width B_0 (m)	Channel depth D_0 (m)	Bed slope S_0 ($\times 10^{-5}$)	River discharge Q_{w0} (m^3/s)	Sediment load Q_{s0} ($\times 10^{-3} m^3/s$)	Sediment grain size d_{50} (μm)	Corresponding single channel
B1-1	0.2	25	200	8	3.05	1,000	2.36	739.82	S1-1
B1-2	0.3	25	200	8	3.05	1,000	3.54	493.21	S1-2
B1-3	0.5	25	200	8	3.05	1,000	5.91	295.93	S1-3
B1-4	1.0	25	200	8	3.05	1,000	11.81	147.96	S1-4
B1-5	1.8	25	200	8	3.05	1,000	21.26	82.20	S1-5
B2-1	0.2	33.33	200	6	4.63	800	2.87	841.75	S2-1
B2-2	0.3	33.33	200	6	4.63	800	4.30	561.17	S2-2
B2-3	0.5	33.33	200	6	4.63	800	7.17	336.70	S2-3
B2-4	1.0	33.33	200	6	4.63	800	14.33	168.35	S2-4
B2-5	1.8	33.33	200	6	4.63	800	25.80	93.53	S2-5

width (B_0') and length (L_0') are 200 and 6,000 m, respectively. As shown in Figures 1f and 1h, the computational domain has a cell size of 40 m in the along-channel direction and consists of 22 cells in the cross-channel direction for the upstream channel (and the single channel) and 10 cells in the cross-channel direction of each bifurcating branch due to the loss of two cells at the bifurcation (see the up-close inset in Figure 1f). As such, the channel widths of the two branches at the bifurcation gradually widened from 90.9 to 100 m in a length of 4 grid cells to attain the same total width between the two branches and the upstream channel following Kleinhans et al. (2008). The same total width results in a constant bed slope between the upstream channel and downstream branches and less affects the equilibrium configuration. As a result, the cell size in cross-channel direction is 9.09 m for the upstream channel (and the single channel) and ranges from 9.09 to 10 m for the two bifurcating branches.

The computational domains consist of upstream boundaries with constant river discharge and an equilibrium sediment load with a uniform sediment grain size, as well as downstream boundaries with a constant water level of the mean sea level (Figures 1e and 1g). The Chezy coefficient (C) was set to $40 m^{1/2}/s$. In this study, Ikeda (1982)'s approach for transverse sediment transport driven by bed-slope effects was adopted with a transverse transport factor $\alpha_{bn} = 10$ following Iwamoto et al. (2020). The computational time step ranges from 0.4 to 0.5 min to ensure the numerical stability and accuracy. The morphological scale factor was adopted in our model to accelerate the morphological evolution and reduce the computational time for long-term morphological simulations (Lesser et al., 2004). In this study, the morphological scale factor ranged from 200 to 1,000, which was varied in different scenarios to avoid intensive in-channel sedimentation in any single computational time step given the different sediment loads at the upstream boundary (Table 1). A spin-up time of 2,880 min was adopted in each scenario to attain fully developed hydrodynamic conditions in the channel network before morphological evolution was allowed. The requirements of a sufficiently small computational time step and morphological scale factor were tested (see Figure S1 in Supporting Information S1).

2.2. Scenario Design

As shown in Table 1, we varied the upstream river discharge Q_{w0} (800 or 1,000 m^3/s), initial water depth D_0 (6 or 8 m), sediment grain size d_{50} (ranging from 82.20 to 841.75 μm), and channel bed slope S_0 (3.05×10^{-5} or 4.63×10^{-5}) for different scenarios, which are mainly derived from natural river deltas with moderate river discharges (Caldwell et al., 2019), such as the Dongjiang Delta (a subdelta of the Pearl River Delta) (Wang et al., 2021) as well as the Hanjiang Delta (Wang et al., 2023) in Guangdong, China and the Po River Delta, Italy (Syvitski et al., 2005) (see also Figure 1). Further, the combinations of the above model settings were adopted to result in moderate Shields stress θ_0 (0.2–1.8) and width-to-depth ratio β_0 ($=B_0/D_0$, 25 or 33.33) of natural river channels (Bolla Pittaluga et al., 2015; Kleinhans & van den Berg, 2011) that attain either symmetric or asymmetric equilibrium configurations of the river bifurcation (Iwamoto et al., 2021).

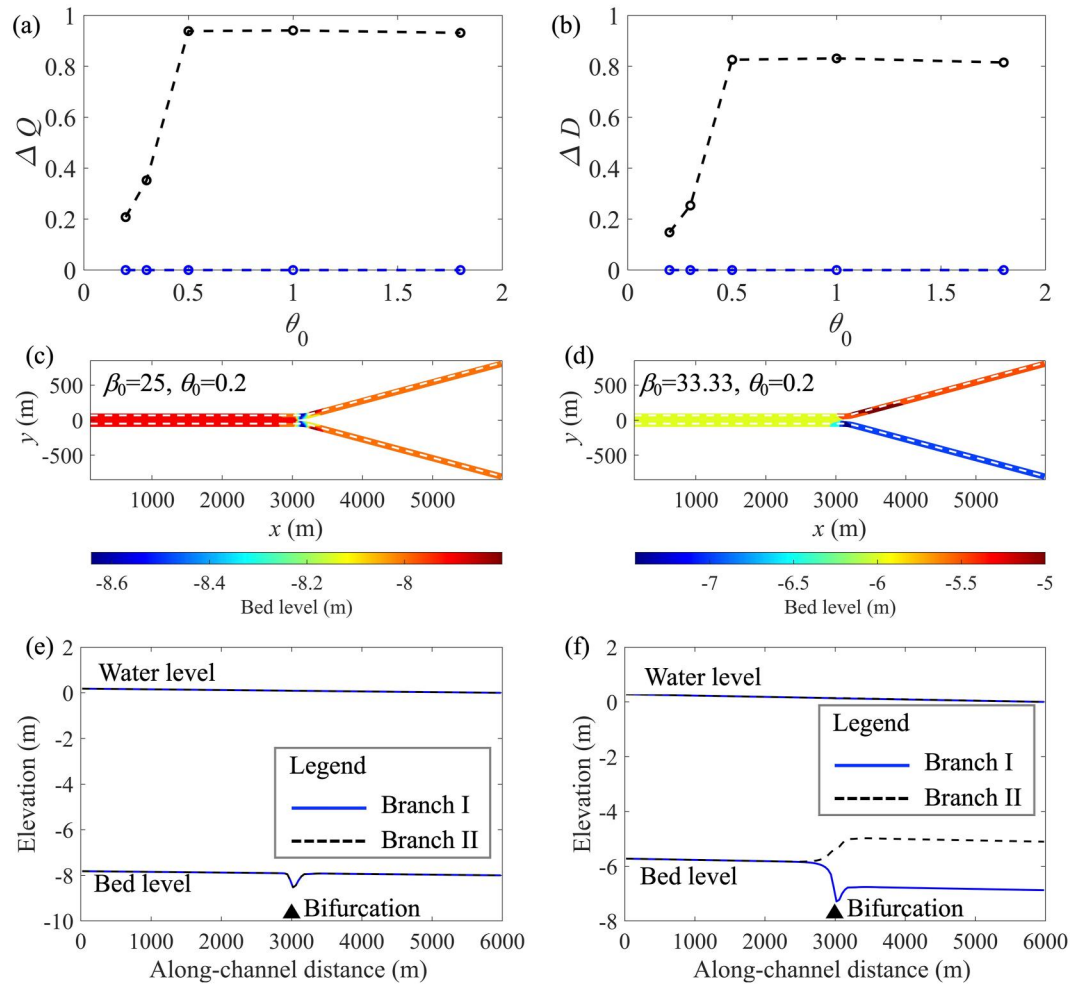


Figure 3. Equilibrium configurations of the river bifurcations for the numerical simulation scenarios in this study: panels (a, b) are the asymmetry of river discharge (ΔQ) and water depth (ΔD) in the two branches in relation to Shields stress θ_0 and width-to-depth ratio β_0 , respectively. Panels (c, d) are the bed levels for representative scenarios of symmetric and asymmetric bifurcations, and panels (e, f) are the water levels and bed levels along the longitudinal profiles indicated by the white dashed lines in panels (c, d).

As shown in Figure 3 (see also Figures S3 and S4 in Supporting Information S1), the initially symmetric bifurcation with a lower bed level by 0.1 or 0.2 m in one of the branches would either recover the symmetric bifurcation or evolve to an asymmetric one, indicating a symmetric or asymmetric equilibrium configuration for the river bifurcation, respectively. The results are consistent with previous studies on the equilibrium configurations of river bifurcations (Bolla Pittaluga et al., 2015; Iwantoro et al., 2021), that is, the increases in θ_0 and β_0 tend to result in an asymmetric bifurcation. In reality, the varying θ_0 and d_{50} can further affect the equilibrium configurations of river bifurcations as they are critical for the transverse sediment transport at the bifurcation (Baar et al., 2018). Notably, the consistent symmetric equilibrium configurations for $\beta_0 = 25$ and the bed ramps at the river bifurcation due to variations of channel width are also reported in the Delft3D simulations of Edmonds and Slingerland (2008). The simulated equilibrium bed levels with either symmetric or asymmetric equilibrium configurations of the river bifurcations were adopted for further simulations with local disturbance of channel deepening (see Figure 2). Notably, in this study, the equilibrium configuration of a single channel is characterized by a linear longitudinal profile given by the water depth D_0 and channel bed slope S_0 (Blom, Arkesteijn, et al., 2017; Gao, Li, et al., 2020). Therefore, the water levels and bed levels are identical for scenarios with constant β_0 , that is, S1-1 to S1-5 for $\beta_0 = 25$ and S2-1 to S2-5 for $\beta_0 = 33.33$, as shown in Figure 4.

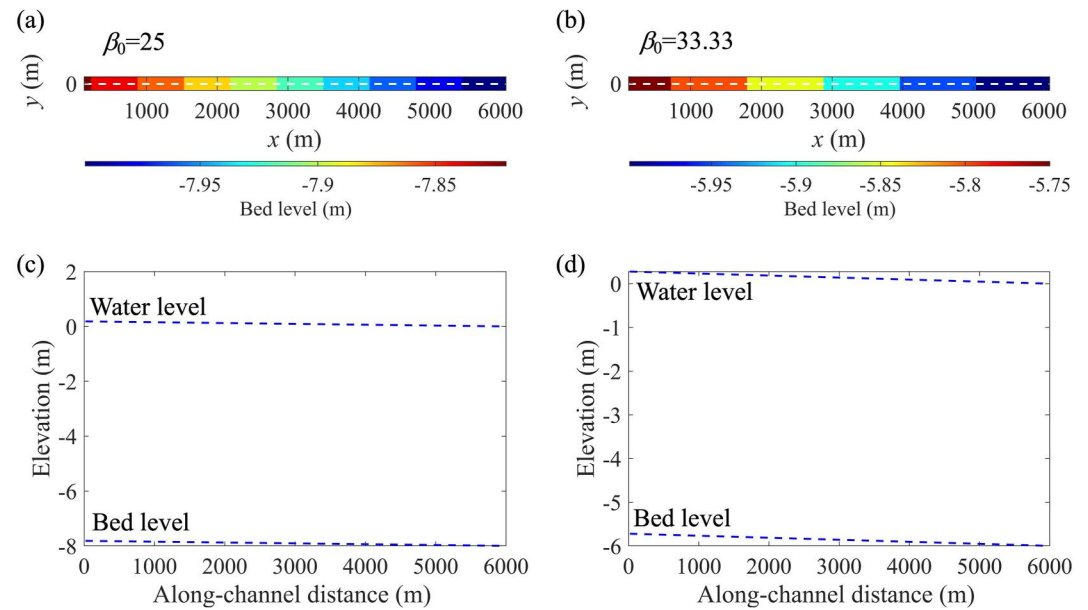


Figure 4. Equilibrium water levels and bed levels for the single channels in this study: panels (a, b) are the bed levels scenarios with different width-to-depth ratio β_0 , and panels (c, d) are the water levels and bed levels along the longitudinal profiles indicated by the white dashed lines in panels (a, b).

As shown in Figures 2a and 2b, the local deepening of borrow-pit due to dredging or sand mining in river channels was added at the halfway of one branch by lowering the bed levels upon the equilibrium bed levels without loss of generality. The length of the borrow-pit L_p is 1,000 m, whereas the depth of the borrow-pit D_p was set to 0.5, 1 and 2 m, resulting in a total removal volume of sand of $0.5\text{--}2 \times 10^5 \text{ m}^3$. We have also conducted additional simulations with different locations and lengths of the borrow-pit, which does not change the conclusion of this study (see Figure S2 in Supporting Information S1). Notably, the local deepening of the borrow-pit was implemented only in branch I when the bifurcation equilibrium is symmetric (i.e., the equilibrium water depths in two branches are the same and hereinafter termed the “symmetric bifurcation”), otherwise the local deepening of the borrow-pit was implemented in either the dominant or the subordinate branch when the bifurcation equilibrium is asymmetric (i.e., the equilibrium water depths in two branches are different and hereinafter termed the “asymmetric bifurcation”) (Figure 3).

For the single channel, we added the borrow-pit at the same along-channel locations with an identical removal sand volume to that in one branch of the channel network. We either created the borrow-pit on the half side of the channel (Figure 2c) or spanning over the cross-section yet with a half-length (Figure 2d) to keep the same volume of sand removal and borrow-pit depth. Therefore, the lengths of the borrow-pits are different in the two configurations.

2.3. Quantifying the Morphological Evolution of Bifurcating Channel Network

To appropriately compare the morphological timescales for different scenarios (Edmonds & Slingerland, 2008), we defined the non-dimensional time T_* as follows:

$$T_* = \frac{t}{D_0 \cdot B_0 \cdot l / Q_{s0}} \quad (2)$$

where t is the elapsed time, l ($=1$ m) is the characteristic length. In this study $D_0 \cdot B_0 \cdot l / Q_{s0}$ indicates the time during which the upstream coming sediment infills a unit length of the channel. Following previous studies (Bolla Pittaluga et al., 2015; Gao et al., 2023), ΔQ was adopted to quantify the asymmetry of water partitioning at the river bifurcation, which reads

$$\Delta Q = \frac{|Q_{w2} - Q_{w1}|}{Q_{w0}} \quad (3)$$

where ΔQ is the river discharge asymmetry, and Q_{w1} and Q_{w2} are the river discharge supplied to branches I and II, respectively. Similarly, we defined the difference in the average water depths of the two branches to show the different morphological configurations in the two branches (Iwantoro et al., 2020) as follows:

$$\Delta D = \frac{|D_2 - D_1|}{D_0} \quad (4)$$

where ΔD is the water depth asymmetry, and D_1 and D_2 are the spatially average water depths in branches I and II, respectively.

To quantify the relative change in river discharge of each branch due to the existence of the borrow-pit, we further defined the relative discharge change dQ as follows:

$$dQ = \frac{Q_{wi} - Q_{wi,e}}{Q_{wi,e}} \quad (5)$$

where $Q_{wi,e}$ is the river discharge in branch I or II when attaining the equilibrium configurations, and the subscript i ($=1$ or 2) indicates branches I and II. Similarly, we adopted the relative slope change dS to quantify the effects of borrow-pit on the water surface slope downstream of the bifurcation in each branch, which reads

$$dS = \frac{S_i - S_{i,e}}{S_{i,e}} \quad (6)$$

where S_i is the water surface slope with the existence of the initial borrow-pit, $S_{i,e}$ is the water surface slope when attaining the equilibrium configurations, and the subscript i ($=1$ or 2) indicates branches I and II. In this study, S_i and $S_{i,e}$ refer to the mean water surface slope between the bifurcation and the upstream end of the initial borrow-pit, since the water surface slope in the upper sections of the two branches is critical to the water partitioning at the bifurcation (Shaw et al., 2021).

In this study, we also theoretically compared the Delft3D simulation results with the phase plane analysis of river bifurcations. Phase plane analysis of river bifurcations indicates the evolution of the water depths in the two branches as the function of the water depths D_1 and D_2 per se (Wang et al., 1995) (see the Supporting Information S1 for the derivation). Furthermore, we quantify the morphological evolution rate of the channel network as follows

$$M = \sqrt{\left(\frac{dD_1}{dt}\right)^2 + \left(\frac{dD_2}{dt}\right)^2} \quad (7)$$

where M is the morphological evolution rate, and dD_1/dt and dD_2/dt are the changing rates of the average water depths in the two branches, respectively. A smaller M indicates a slower morphological evolution of the channel network, and vice versa.

3. Results

3.1. Channel Responses to Local Disturbance

Figure 5 shows the temporal and spatial evolution of channel networks with local disturbances in one of the branches. For different bifurcations with symmetric or asymmetric equilibrium configurations, we found that the evolution of bed levels with local disturbance can be largely divided into two stages (Figures 5a and 5d): For *Stage I*: The initial pit is infilled and migrates downstream while the entire branch is uniformly eroded (Figures 5b and 5e). At the same time, a deposition wave originated at the river bifurcation propagates downstream in the other branch, leading to uniform siltation of the entire branch (Figures 5b and 5e). The siltation in the other branch can

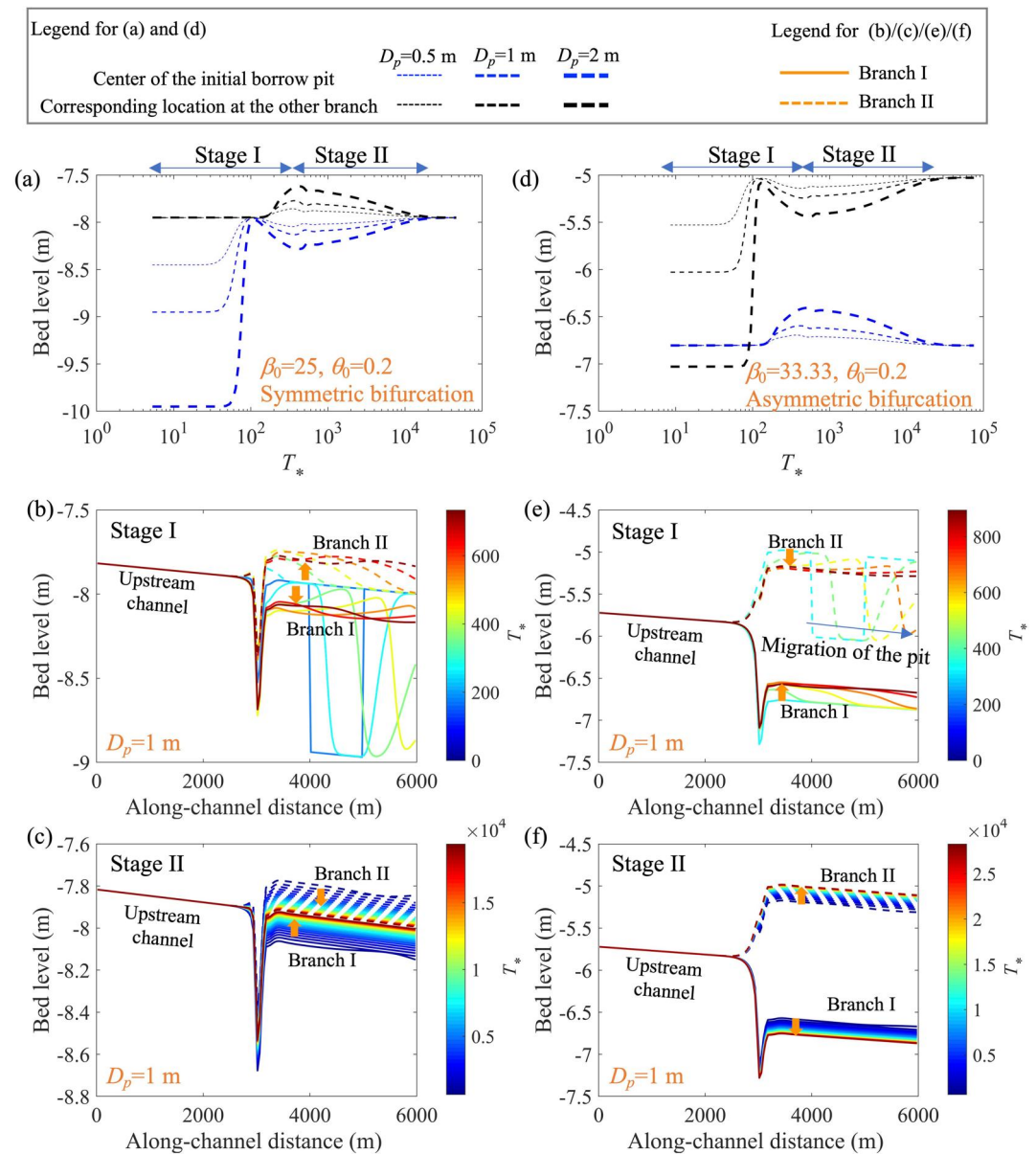


Figure 5. The temporal evolution of the bed levels at the center of the initial borrow-pits and the corresponding location in the other branch for (a) symmetric and (b) asymmetric bifurcations with different depths of the borrow-pits D_p . The initial borrow pits locate at branch I and branch II for (a) symmetric and (b) asymmetric bifurcations, respectively. Panels (b, c, e, f) are the temporal evolution of the longitudinal profiles during stages I and II corresponding to scenarios in panels (a, d), respectively, with $D_p = 1$ m. The line color in panels (b, c, e, f) scales with the non-dimensional time T_* .

be considered as a “system-wide effect” of the local disturbance in this study. As for *Stage II*: The bed levels of the two branches subsequently recover the initial equilibrium configurations while largely maintaining linear profiles (except the bed ramps at the bifurcation) (Figures 5c and 5f).

We also found that the timescale for recovering the equilibrium configuration (stage II) is much longer than the initial infilling of the borrow-pits (stage I) (Figures 5a and 5d). Furthermore, the magnitude of the erosion/siltation in the two entire branches tends to decrease with decreasing initial depth of the borrow-pit (Figures 5a and 5d). The above processes are persistent for scenarios with different Shields stress θ_0 and different locations of initial borrow-pit in the dominant or subordinate branch (see Figures S5 and S6 in Supporting Information S1). Notably, in this study, the bed levels of the upstream channel are not affected by the local disturbance (Figures 5b, 5c, 5e, and 5f).

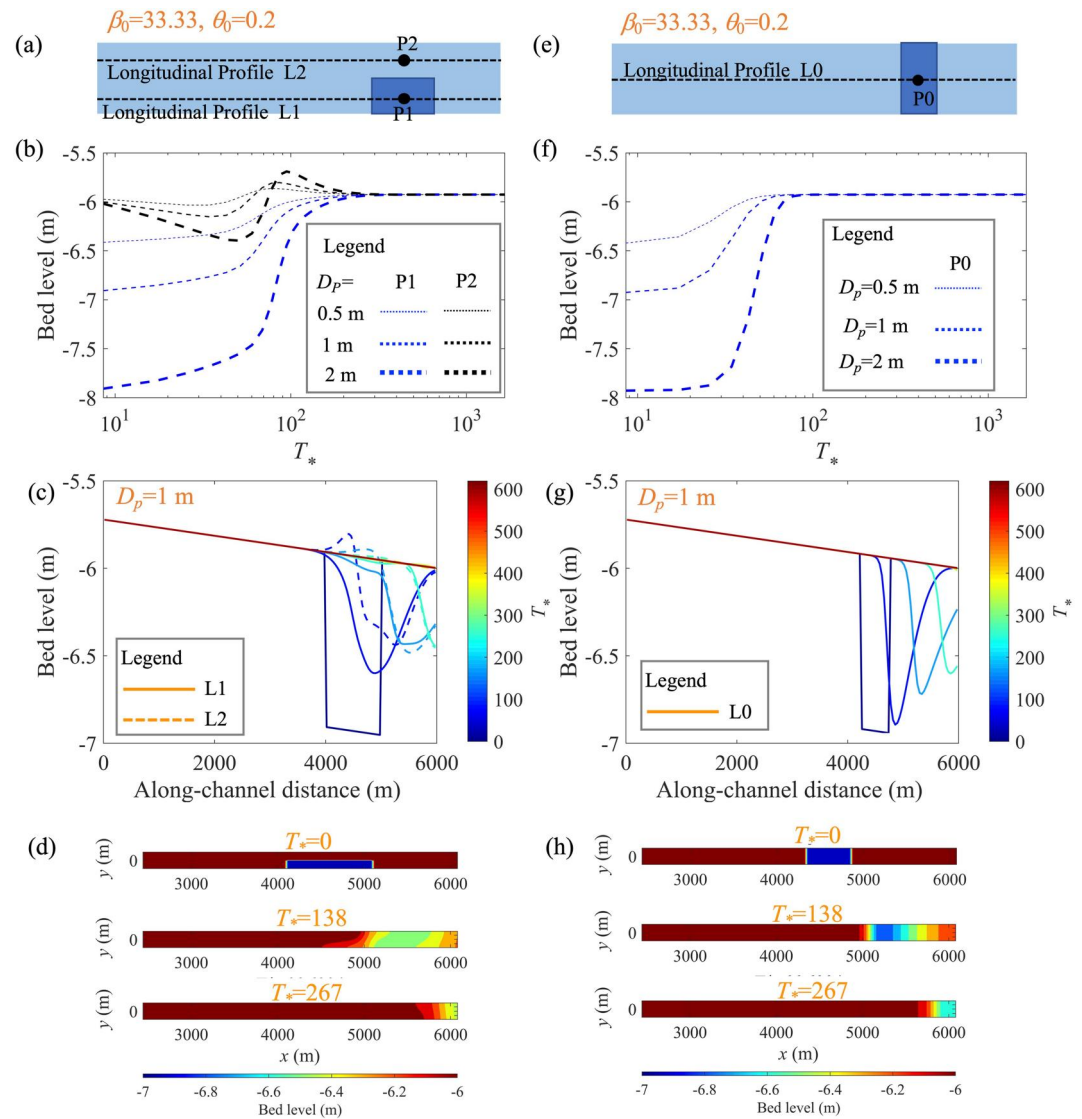


Figure 6. Panels (a, e) show different scenarios of borrow-pits (the dark blue area) in a single channel. Panels (b, c, f, g) are the temporal evolution of the bed levels at representative locations (P0, P1, and P2) and longitudinal profiles (L0, L1, and L2) for the scenarios shown in panels (a, e), respectively. Panels (d, h) are the spatial evolution of the bed levels at representative time instants for scenarios shown in panels (a, e), respectively. The representative locations (P0, P1, and P2) and longitudinal profiles (L0, L1, and L2) are indicated as the black dots and dashed lines, respectively, in panels (a, e). The line color in panels (c, g) scales with the non-dimensional time T_* . D_p is the depth of the initial borrow-pit.

For a single channel, the borrow-pit is rapidly infilled when propagating downstream (Figure 6), which is consistent with previous studies (Barman et al., 2020; Haghazari et al., 2020). When the initial borrow-pit only occupies half side of the river channel (Figure 2c), the pit expands in the cross-channel direction when propagating downstream (Figure 6d). Further, the morphological timescale for recovering the equilibrium configuration in a single channel is relatively short compared with that in a channel network (Figure 5).

Figure 7 shows the water partitioning at the bifurcation over time as well as its asymmetry for representative scenarios (see Figures S7 and S8 in Supporting Information S1 for other scenarios). As expected, the river discharge of the eroded branch (where the initial borrow-pit located) first increases during stage I and then approaches the equilibrium discharge during stage II, and vice versa in the silted branch. Furthermore, the increased river discharge in the eroded branch during stage I is larger with increasing depth of the initial borrow-pit.

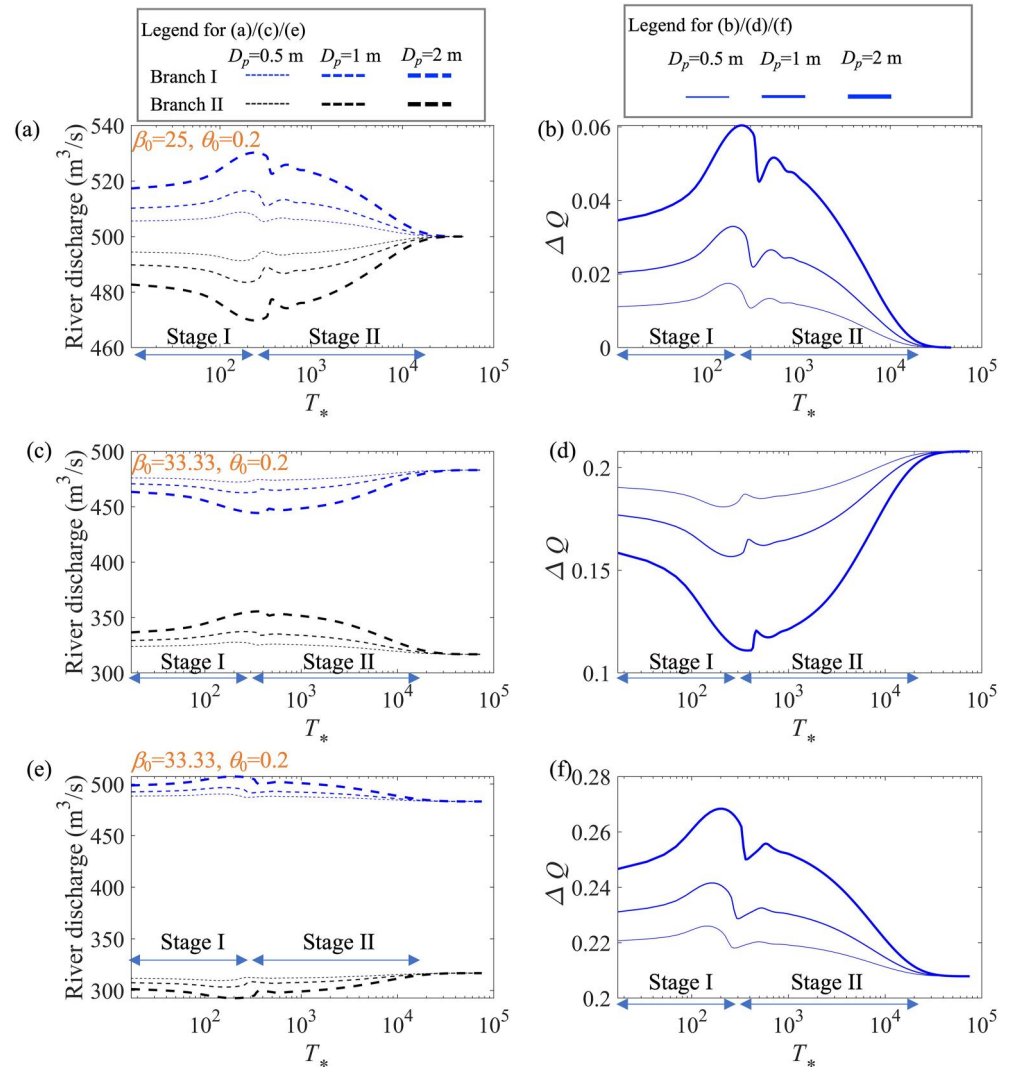


Figure 7. Water partitioning at the bifurcation and its asymmetry over time for representative scenarios with different equilibrium configurations of river bifurcations and locations of the borrow-pit: panels (a, b) are symmetric bifurcation with the borrow-pit in branch I; panels (c, d) are asymmetric bifurcation with the borrow-pit in the subordinate branch (i.e., branch II); and panels (e, f) are asymmetric bifurcation with the borrow-pit in the dominant branch (i.e., branch I).

3.2. Morphological Timescales of the Channel Responses

We quantified the nondimensional timescales of the two stages by detecting the time instants when the eroded branches convey their maximum river discharge (T_{*1}) and the time instants when the branch recovers the equilibrium discharge (T_{*2}). As shown in Figure 8a, T_{*1} tends to increase with increasing depth of the borrow-pits, which is due to the increasing time for infilling the increasing volume of the borrow-pits. Further, for an asymmetric bifurcation, T_{*1} tends to be greater when the borrow-pits are located in the subordinate branch with a relatively lower river discharge Q_{wp}/Q_{w0} (Figure 8b). Here, Q_{wp} is the equilibrium river discharge in the branch with the initial borrow-pit and Q_{w0} is the upstream discharge. As shown in Figure 8c, while T_{*2} tends to increase with increasing depth of the borrow-pits, it does not show a significant difference between different scenarios with symmetric or asymmetric bifurcations in this study. Furthermore, we found that the timescale for the branches to recover the equilibrium discharge (T_{*2}) can be up to 370 times longer than T_{*1} , and T_{*2}/T_{*1} tends to increase with increasing Q_{wp}/Q_{w0} (Figure 8d). The differences between T_{*1} and T_{*2} are discussed in Section 4.2.

Notably, when the initial borrow-pits are located in the dominant branch of a highly asymmetric bifurcation (Scenarios B2-3 to B2-5), the alterations in the water partitioning at the bifurcation can be negligible due to the

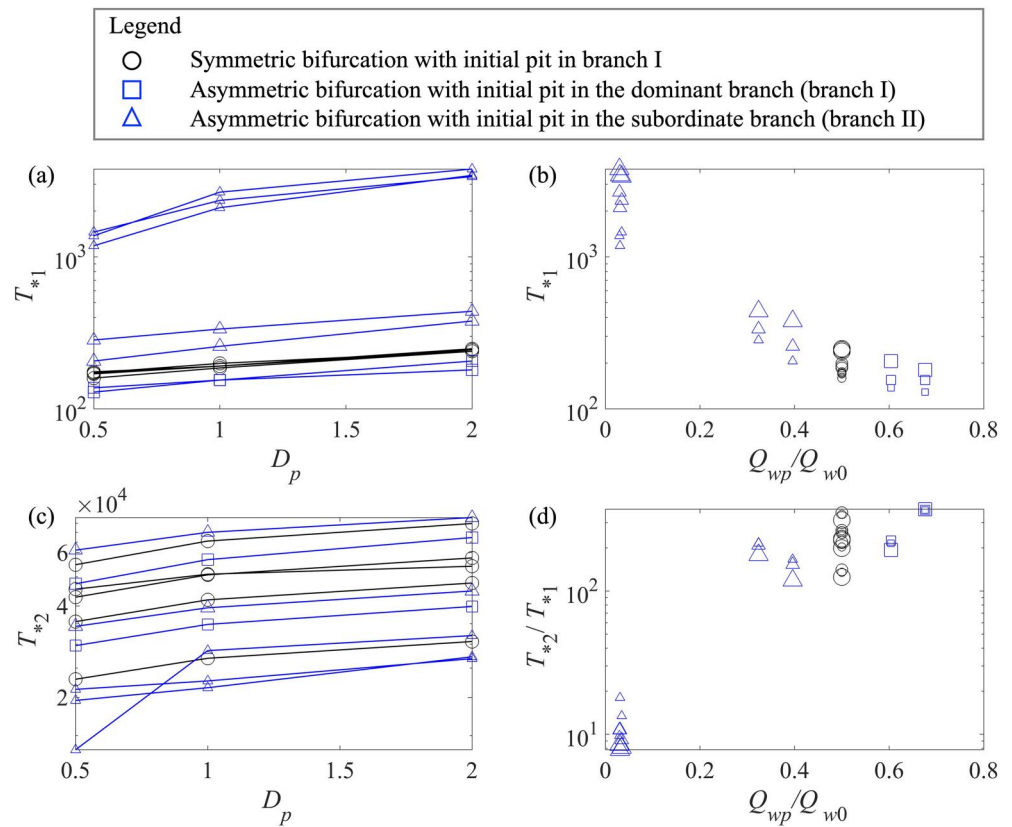


Figure 8. Nondimensional timescale for the infilling of the initial borrow-pits (i.e., stage I) T_{*1} against (a) the depth of the initial borrow-pit D_p and (b) the relative discharge in the branch with the initial borrow-pit Q_{wp}/Q_{w0} . Panel (c) is the nondimensional timescale for the recovery of the equilibrium discharges (i.e., stage II) T_{*2} against the depth of the initial borrow-pit D_p , and panel (d) shows T_{*2}/T_{*1} against Q_{wp}/Q_{w0} . Q_{wp} is the equilibrium river discharge in the branch with the initial borrow-pit and Q_{w0} is the upstream discharge. The symbol sizes scale with Q_{wp}/Q_{w0} for panels (a, c) and scale with D_p for panels (b, d).

larger water depth and the rapid infilling of the initial borrow-pits with the high sediment supply in the branch (see Figure S6 in Supporting Information S1). This result is consistent with existing physical experiments (Lee et al., 1993), which showed that increasing sediment transport capacity can lead to increasing downstream migration rate of initial borrow-pits and hence the rapid infilling. In such cases, the effects of the burrow-pit on the morphological evolution of the channel network are negligible. As such, T_{*1} and T_{*2} tend to be relatively small and are thus not included in Figure 8.

4. Discussion

4.1. Mechanism Leading to the System-Wide Effects

In this study, we found that the local deepening in one branch of a bifurcating channel network can lead to system-wide effects. Specifically, in the initial stage (i.e., stage I) erosion occurs in the entire branch with the local deepening, whereas siltation occurs in the other branch. In the following section, we further illustrated the mechanism leading to the erosion/siltation in the two branches during stage I. Figure 9 shows the initial water levels in the channel networks with the existence of the borrow-pits as well as the water levels when recovering the equilibrium configurations for representative scenarios. For the channel network of river bifurcation, the existence of the borrow-pit tends to increase the water surface slope downstream of the bifurcation in the branch with local deepening compared with the other branch (see the solid blue lines in Figures 9b and 9c). The increased water surface slope thus increases the river discharge in the branch (Figure 7) and leads to the further erosion of the branch during stage I (Figure 5). Also, the decreased river discharge in the other branch leads to its siltation (Figure 5). Nonetheless, the water depths in the two branches will eventually recover their equilibrium

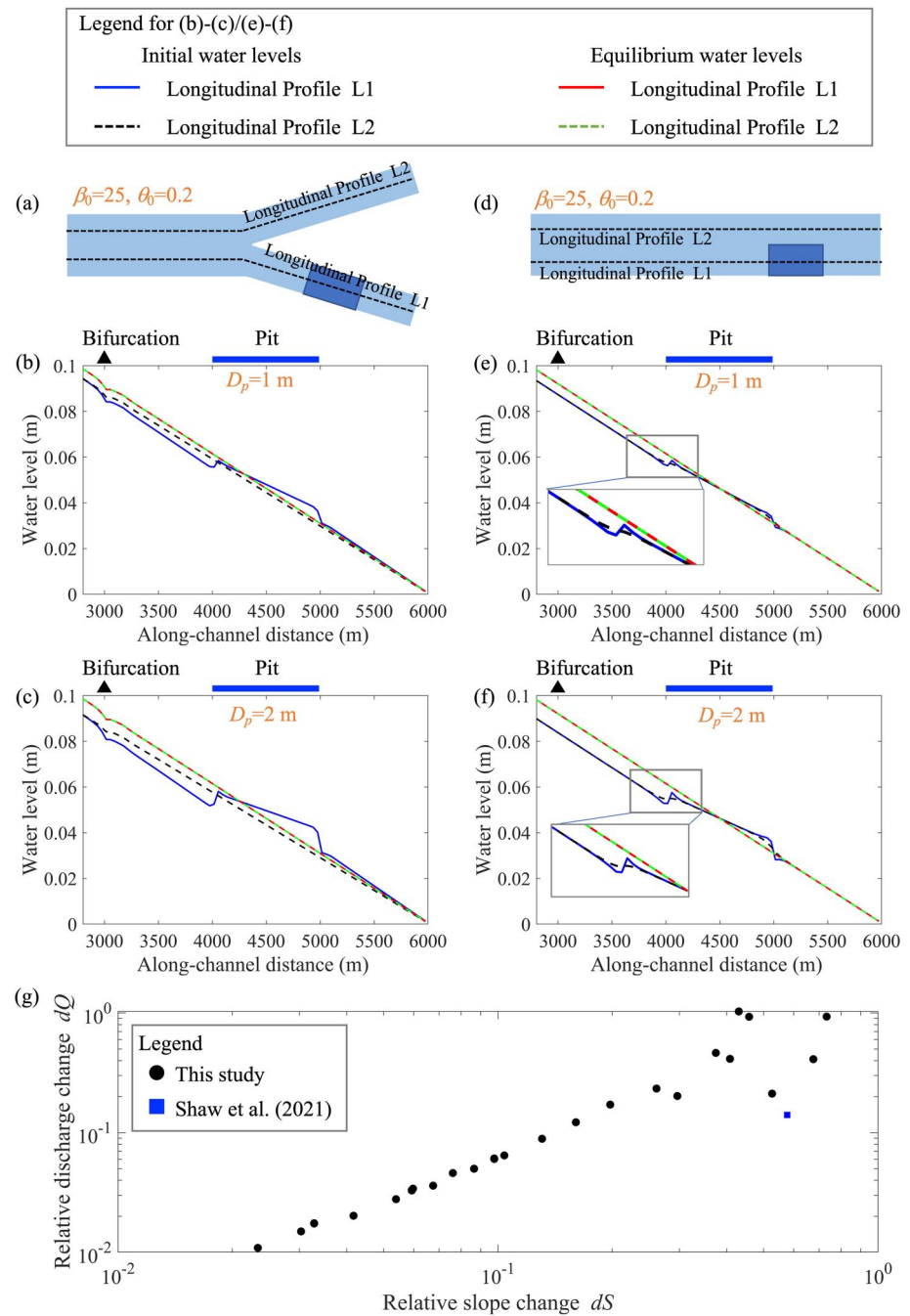


Figure 9. The schematized locations of the borrow-pits for representative scenarios of (a) symmetric bifurcation and (d) single channel. Panels (b, c, e, f) are the longitudinal profiles of the initial and equilibrium water levels for scenarios shown in panels (a, d), respectively, with different depths of the initial borrow-pit D_p . The locations of the longitudinal profiles (L1 and L2) in panels (b, c, e, f) are indicated as the black dashed lines in panels (a, d), respectively. Panel (g) shows the relationship between the relative discharge change dQ and the relative slope change dS in the branch with the initial borrow-pit.

configurations during stage II yet with a longer timescale (Figures 5 and 8). As shown in Figure 9g, the relative discharge change dQ (Equation 5) in the branch with the borrow-pit at T_{*1} (Figure 7), that is, the maximum dQ , tends to increase with increasing relative slope change dS (Equation 6). In this study, the relative slope change dS and the relative discharge change dQ can reach up to 0.73 and 1.03, respectively.

Essentially, in this study the erosion/siltation in the two branches during the initial stage (stage I) results from the alterations of water levels at the bifurcation due to the existence of the borrow-pits. The variations in water levels further change the water and sediment supplies to the two branches, which therefore leads to the morphological evolution in both branches and drives the bifurcation away from its equilibrium configurations. Therefore, the system-wide effects of local disturbance are essentially due to the alterations in the water partitioning at the river bifurcation. The system-wide effects of the local disturbance on the water surface slope have also been reported in the Mississippi-Atchafalaya bifurcation (Shaw et al., 2021), which showed that the dredging in the lower Atchafalaya River led to the increased water surface slope in its upstream reach and hence the increased river discharge in the Atchafalaya River through the Mississippi-Atchafalaya bifurcation. The relative slope change dS and relative discharge change dQ due to dredging in Shaw et al. (2021) were estimated to be 0.58 and 0.14, respectively, which fall in the ranges of our simulations (see the blue rectangle in Figure 9g). Nonetheless, the comparison with Shaw et al. (2021) is qualitative as the river discharge and channel geometry of the Mississippi-Atchafalaya bifurcation are much larger than in our simulations.

In a single channel with a local deepening at half side of the river channel (Figure 9d), we also found the drawdown of the water levels (Figures 9e and 9f). Nonetheless, the differences in the water levels between the two representative longitudinal profiles in a single channel only locally occur at the two along-channel ends of the borrow-pits. The limited difference in water levels is presumably due to the momentum transfer in the cross-channel direction (Proust et al., 2009). In contrast, the differences in the water levels can persist in the two bifurcating branches due to the separation of the water body (Edmonds & Slingerland, 2008). The results suggest that the restoration of side channels or the construction of longitudinal training walls in river channels can lead to different hydrodynamic development and morphological evolution in the two branches (Le et al., 2018; van Denderen et al., 2018).

4.2. Comparison With Theoretical Analyses

The relatively long timescales for stage II (i.e., the recovery to the equilibrium configurations) were theoretically compared with the phase plane analysis (Wang et al., 1995). Figures 10a and 10c show the evolution rate of river bifurcation (M) as a function of the water depths of the two branches (D_1 and D_2) for representative scenarios of symmetric and asymmetric bifurcations using phase plane analysis. As shown in Figures 10b and 10d, we further compared the Delft3D simulations of the morphological evolution of the channel network with the theoretical analyses of the phase plane during stage II when the water depths in each branch are constant. The evolution trajectory of water depths of the two branches are consistent between the theoretical predictions (white dashed lines in Figures 10b and 10d) and the Delft3D simulations (red lines Figures 10b and 10d). Further, we found a “slowing zone” on the phase plane where the evolution rate of the river bifurcation M is relatively low (Figures 10a and 10c). The low evolution rate of water depths at the vicinity of the equilibrium configurations also explains the longer timescales (T_{*2}) for the branches to recover the equilibrium configurations and discharges.

The decreasing morphological evolution rate of a bifurcating channel network when approaching the equilibrium configuration is also found in the one-dimensional simulations of Iwamoto et al. (2020). Further, the relatively long timescale (T_{*2}) for the branches to recover the equilibrium configurations due to the existence of the “slowing zone” could also explain the less significant difference in T_{*2} between different scenarios with symmetric and asymmetric bifurcations. Specifically, T_{*2} is largely determined by the timescale to pass through the “slowing zone.”

4.3. Implications for Evolution and Management of Channel Networks

Channel networks benefit coastal communities in numerous aspects, such as water supplies and navigation. In this study we found that the local disturbance can lead to long-term and system-wide morphological responses in channel networks (Figure 5). Furthermore, the system-wide morphological responses pertain to the “process connectivity” in deltaic channel networks (Passalacqua, 2017), that is, the bed changes in one of the branches are highly coupled with the other branch. Therefore, it is critical to explore the long-term morphological responses to human intervention in the entire channel network rather than focusing on a single channel reach (Chowdhury et al., 2023; Cox et al., 2021; Wang et al., 2022). The long timescale for recovering the equilibrium (Figures 5

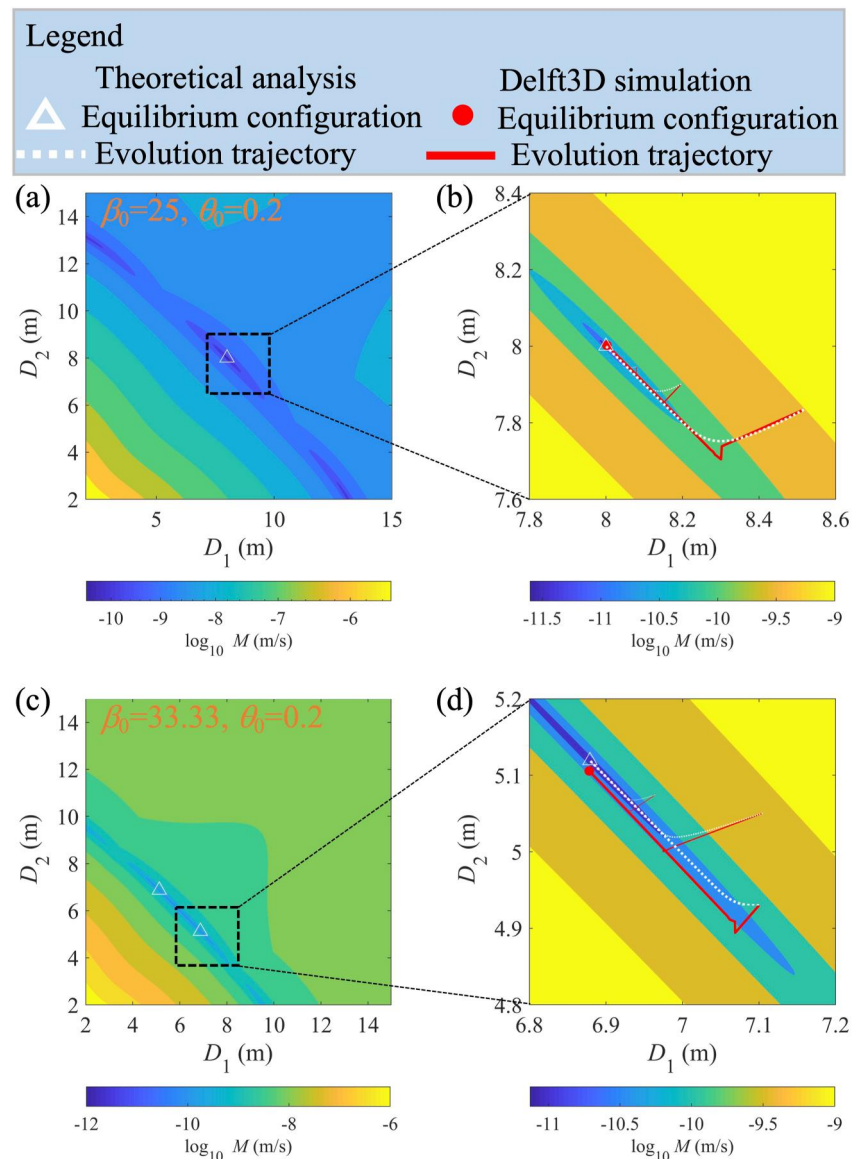


Figure 10. The evolution rate of water depths M in relation to the water depths in the two branches (D_1 and D_2) per se and the equilibrium configurations of water depths for representative scenarios of (a) symmetric and (c) asymmetric bifurcations. Panels (b, d) are up-close looks that show the evolution trajectories of water depths when approaching their equilibrium configurations predicted by the phase plane analyses and the Delft3D simulations.

and 7) can lead to significantly cumulative alterations of the water and material supplies to the downstream habitats (Hariharan et al., 2023).

With the intensive human intervention in the many deltas across the world, our results can also help understand the long-term morphological evolution of the channel network and inform the mitigation of the relevant hazards and risks, such as salt water intrusion, flooding and river avulsion (Cox et al., 2021; Luo et al., 2007; Shaw et al., 2021; Wang et al., 2015). For example, the spatially uneven navigation dredging and sand mining in the channel network of the Pearl River Delta and the Yangtze River Estuary have led to the alterations of the water partitioning at the bifurcations (Chen et al., 2022; Luo et al., 2007; Wang et al., 2022), which can potentially affect the spatial patterns of salt water intrusion and flood risks (Biemond et al., 2023; Qiu et al., 2022). The dredging activities in the lower Atchafalaya River have resulted in an altered water partition at the Mississippi-Atchafalaya bifurcation (Shaw et al., 2021). Specifically, the river discharge increased in the Atchafalaya River after the local

dredging in its lower reach between 1932 and 1950 in addition to channel erosion; the increased river discharge partitioning to the Atchafalaya has caused concerns on the potential abandonment of the lower Mississippi River (Fisk, 1952; Shaw et al., 2021). Although our study suggests that the silted branch would eventually recover the equilibrium configuration with a larger water depth (Figure 5), the prolonged recovery could increase its risk of closing-off given the decreasing water discharge and shallower water depth (Riquier et al., 2017; Slingerland & Smith, 1998).

Notably, this study was conducted in a simple bifurcating channel network with identical lengths and widths of the two branches. In complex channel networks with multiple bifurcations in natural deltas, the water and sediment partitioning at bifurcations are highly coupled in the channel network, potentially leading to emergent behavior on the bifurcation equilibrium configurations (Ragno et al., 2022; Salter et al., 2020). Furthermore, the bifurcation equilibrium configurations can also be affected by tides, waves, sea-level rise, salinity, changing river discharge, backwaters and river mouth progradation (Buschman et al., 2013; Edmonds, 2012; Edmonds et al., 2010; Gao et al., 2018; Hariharan et al., 2022; Iwantoro et al., 2022; Salter et al., 2018) as well as the channel geometry, such as meandering and changing channel width and length (Redolfi et al., 2019). The propagation of the local disturbance in such a large-scale complex channel network is worth exploring in the future as the recovery to the equilibrium configuration could differ from a single bifurcation.

5. Conclusions

In this study, we explored the responses of a bifurcating channel network (i.e., a river bifurcation with an upstream channel and two branches) to local disturbance of channel deepening such as borrow-pits due to dredging or sand mining. The results were further compared with scenarios with a single channel as well as theoretical analyses on the evolution of river bifurcations. Main conclusions are listed as follows:

1. The responses of bifurcating channel networks to local disturbance of channel deepening show patterns widely different from a single channel. While the recovery of the bed level is rapid in a single channel, the responses of the channel network can be divided into two stages:
Stage I: The rapid infilling of the local disturbance of channel deepening is associated with the erosion of the entire branch, which also causes system-wide effects on the siltation in the other branch.
Stage II: The eroded and silted branches then gradually recover their initial symmetric/asymmetric equilibrium configurations.
2. The erosion/siltation of the two branches during stage I is due to the variations in water levels of the two branches that alter the water partitioning at the bifurcation.
3. While the infilling of the local disturbance of channel deepening during stage I is relatively rapid, the recovery of the equilibrium configurations during stage II is much slower.
4. The long timescales for recovering the equilibrium configurations are theoretically consistent with phase plane analyses, which show a “slowing zone” for the morphological evolution of the two branches when approaching the equilibrium configurations.

Our results show that the responses of a channel network to local disturbances are more complex than that of a single channel. The local disturbances in one branch can lead to long-term system-wide effects on the morphological evolution of the entire channel network. Our results suggest the importance of exploring the long-term morphological responses of the entire channel network rather than a single channel reach, which also benefits the design and management of channel network restorations. Future studies can further relax the simplification of the channel network and the local disturbance, such as considering the different lengths, channel widths and meandering of the two branches as well as incorporating scenarios with different locations and magnitudes of the local disturbance. The propagation of the local disturbances in complex channel networks with multiple bifurcations under tides, sea-level rise, changing river discharge, river mouth progradation, etc. is also worth exploring in the future.

Data Availability Statement

The Delft3D model setup files and the code for phase plane analysis are available on the Zenodo database Gao (2023) (<https://doi.org/10.5281/zenodo.8362570>).

Acknowledgments

This work was supported by the National Natural Science Foundation of China (Grants 52388101, 52239005, and 52101297) and the Program for Guangdong Introducing Innovative and Entrepreneurial Teams (Grant 2019ZT08L213). D. Shao acknowledged the support from the National Key R&D Program of China (Grant 2019YFE0121500).

References

Anthony, E. J., Brunier, G., Besset, M., Goichot, M., Dussouillez, P., & Nguyen, V. L. (2015). Linking rapid erosion of the Mekong River delta to human activities. *Scientific Reports*, 5(1), 14745. <https://doi.org/10.1038/Srep14745>

Baar, A. W., de Smit, J., Uijtewaal, W. S. J., & Kleinhans, M. G. (2018). Sediment transport of fine sand to fine gravel on transverse bed slopes in rotating annular flume experiments. *Water Resources Research*, 54(1), 19–45. <https://doi.org/10.1002/2017WR020604>

Barman, B., Sarma, A. K., & Kumar, B. (2020). Mining pit migration of an alluvial channel: Experimental and numerical investigations. *ISH Journal of Hydraulic Engineering*, 26(4), 448–456. <https://doi.org/10.1080/09715010.2018.1501775>

Best, J. (2019). Anthropogenic stresses on the world's big rivers. *Nature Geoscience*, 12(1), 7–21. <https://doi.org/10.1038/s41561-018-0262-x>

Biamond, B., de Swart, H. E., & Dijkstra, H. A. (2023). Mechanisms of salt overspill at estuarine network junctions explained with an idealized model. *Journal of Geophysical Research: Oceans*, 128(3), e2023JC019630. <https://doi.org/10.1029/2023JC019630>

Blom, A., Arkesteijn, L., Chavarrías, V., & Viparelli, E. (2017). The equilibrium alluvial river under variable flow and its channel-forming discharge. *Journal of Geophysical Research: Earth Surface*, 122(10), 1924–1948. <https://doi.org/10.1002/2017jf004213>

Blom, A., Chavarrías, V., Ferguson, R. I., & Viparelli, E. (2017). Advance, retreat, and halt of abrupt gravel-sand transitions in Alluvial Rivers. *Geophysical Research Letters*, 44(19), 9751–9760. <https://doi.org/10.1002/2017gl074231>

Blom, A., Viparelli, E., & Chavarrías, V. (2016). The graded alluvial river: Profile concavity and downstream fining. *Geophysical Research Letters*, 43(12), 6285–6293. <https://doi.org/10.1002/2016gl068898>

Bolla Pittaluga, M., Coco, G., & Kleinhans, M. G. (2015). A unified framework for stability of channel bifurcations in gravel and sand fluvial systems. *Geophysical Research Letters*, 42(18), 7521–7536. <https://doi.org/10.1002/2015GL065175>

Bolla Pittaluga, M., Repetto, R., & Tubino, M. (2003). Channel bifurcation in braided rivers: Equilibrium configurations and stability. *Water Resources Research*, 39(3). <https://doi.org/10.1029/2001WR001112>

Buschman, F. A., van der Vegt, M., Hoitink, A. J. F., & Hoekstra, P. (2013). Water and suspended sediment division at a stratified tidal junction. *Journal of Geophysical Research: Oceans*, 118(3), 1459–1472. <https://doi.org/10.1002/jgrc.20124>

Caldwell, R. L., Edmonds, D. A., Baumgardner, S., Paola, C., Roy, S., & Nienhuis, J. H. (2019). A global delta dataset and the environmental variables that predict delta formation. *Earth Surface Dynamics*, 7(3), 773–787. <https://doi.org/10.5194/esurf-7-773-2019>

Chang, H. H. (1986). River channel changes: Adjustments of equilibrium. *Journal of Hydraulic Engineering*, 112(1), 43–55. [https://doi.org/10.1061/\(ASCE\)0733-9429\(1986\)112:1\(43\)](https://doi.org/10.1061/(ASCE)0733-9429(1986)112:1(43))

Chen, D., Acharya, K., & Stone, M. (2010). Sensitivity analysis of nonequilibrium adaptation parameters for modeling mining-pit migration. *Journal of Hydraulic Engineering*, 136(10), 806–811. [https://doi.org/10.1061/\(ASCE\)HY.1943-7900.0000242](https://doi.org/10.1061/(ASCE)HY.1943-7900.0000242)

Chen, X. Q., Yu, M. H., Liu, C. J., Wang, R. P., Zha, W., & Tian, H. Y. (2022). Topological and dynamic complexity of the Pearl River Delta and its responses to human intervention. *Journal of Hydrology*, 608, 127619. <https://doi.org/10.1016/j.jhydrol.2022.127619>

Chowdhury, M. K., Blom, A., Ylla Arbós, C., Verbeek, M. C., Schropp, M. H. I., & Schielen, R. M. J. (2023). Semicentennial response of a bifurcation region in an engineered river to peak flows and human interventions. *Water Resources Research*, 59(4), e2022WR032741. <https://doi.org/10.1029/2022WR032741>

Cox, J. R., Huismans, Y., Knaake, S. M., Leuven, J. R. F. W., Vellinga, N. E., van der Vegt, M., et al. (2021). Anthropogenic effects on the contemporary sediment budget of the lower Rhine-Meuse delta channel network. *Earth's Future*, 9(7), e2020EF001869. <https://doi.org/10.1029/2020EF001869>

Doyle, M. W., & Harbor, J. M. (2003). A scaling approximation of equilibrium timescales for sand-bed and gravel-bed rivers responding to base-level lowering. *Geomorphology*, 54(3), 217–223. [https://doi.org/10.1016/S0169-555X\(02\)00357-4](https://doi.org/10.1016/S0169-555X(02)00357-4)

Edmonds, D., Slingerland, R., Best, J., Parsons, D., & Smith, N. (2010). Response of river-dominated delta channel networks to permanent changes in river discharge. *Geophysical Research Letters*, 37(12), L12404. <https://doi.org/10.1029/2010GL043269>

Edmonds, D. A. (2012). Stability of backwater-influenced river bifurcations: A study of the Mississippi-Atchafalaya system. *Geophysical Research Letters*, 39(8), L08402. <https://doi.org/10.1029/2012gl015125>

Edmonds, D. A., Chadwick, A. J., Lamb, M. P., Lorenzo-Trueba, J., Murray, A. B., Nardin, W., et al. (2021). *Morphodynamic modeling of river-dominated deltas: A review and future perspectives reference module in earth systems and environmental sciences*. Elsevier.

Edmonds, D. A., & Slingerland, R. L. (2008). Stability of delta distributary networks and their bifurcations. *Water Resources Research*, 44(9). <https://doi.org/10.1029/2008WR006992>

Englund, F., & Hansen, E. (1967). *A monograph on sediment transport in alluvial streams*. Teknisk Forlag.

Eslami, S., Hoekstra, P., Nguyen Trung, N., Ahmed Kantoush, S., Van Binh, D., Duc Dung, D., et al. (2019). Tidal amplification and salt intrusion in the Mekong Delta driven by anthropogenic sediment starvation. *Scientific Reports*, 9(1), 18746. <https://doi.org/10.1038/s41598-019-55018-9>

Ferrer-Boix, C., Chartrand, S. M., Hassan, M. A., Martín-Vide, J. P., & Parker, G. (2016). On how spatial variations of channel width influence river profile curvature. *Geophysical Research Letters*, 43(12), 6313–6323. <https://doi.org/10.1002/2016gl069824>

Fisk, H. N. (1952). *Geological investigation of the Atchafalaya basin and the problem of Mississippi river diversion*. US Army Corps of Engineers.

Gao, W. (2023). System-wide effects of local bed disturbance on the morphological evolution of a bifurcating channel network. *Zenodo*. <https://doi.org/10.5281/zenodo.8362570>

Gao, W., Li, D., Wang, Z. B., Nardin, W., Shao, D., Sun, T., et al. (2020). The longitudinal profile of a prograding river and its response to sea level rise. *Geophysical Research Letters*, 47(21), e2020GL090450. <https://doi.org/10.1029/2020gl090450>

Gao, W., Nienhuis, J., Nardin, W., Wang, Z. B., Shao, D., Sun, T., & Cui, B. (2020). Wave controls on deltaic shoreline-channel morphodynamics: Insights from a coupled model. *Water Resources Research*, 56(9), e2020WR027298. <https://doi.org/10.1029/2020wr027298>

Gao, W., Shao, D., Wang, Z. B., Nardin, W., Yang, W., Sun, T., & Cui, B. (2018). Combined effects of unsteady river discharges and wave conditions on river mouth bar morphodynamics. *Geophysical Research Letters*, 45(23), 12903–12911. <https://doi.org/10.1029/2018GL080447>

Gao, W., Wang, Z. B., Kleinhans, M. G., Miao, C., Cui, B., & Shao, D. (2023). Floodplain connecting channels as critical paths for hydrological connectivity of deltaic river networks. *Water Resources Research*, 59(4), e2022WR033714. <https://doi.org/10.1029/2022WR033714>

Haghnazar, H., Sangsefidi, Y., Mehraein, M., & Tavakol-Davani, H. (2020). Evaluation of infilling and replenishment of river sand mining pits. *Environmental Earth Sciences*, 79(14), 362. <https://doi.org/10.1007/s12665-020-09106-z>

Hariharan, J., Passalacqua, P., Xu, Z., Michael, H. A., Steel, E., Chadwick, A., et al. (2022). Modeling the dynamic response of river deltas to sea-level rise acceleration. *Journal of Geophysical Research: Earth Surface*, 127(9), e2022JF006762. <https://doi.org/10.1029/2022JF006762>

Hariharan, J., Wright, K., Moodie, A., Tull, N., & Passalacqua, P. (2023). Impacts of human modifications on material transport in deltas. *Earth Surface Dynamics*, 11(3), 405–427. <https://doi.org/10.5194/esurf-11-405-2023>

Hoitink, A. J. F., Nittrouer, J. A., Passalacqua, P., Shaw, J. B., Langendoen, E. J., Huismans, Y., & van Maren, D. S. (2020). Resilience of river deltas in the Anthropocene. *Journal of Geophysical Research: Earth Surface*, 125(3), e2019JF005201. <https://doi.org/10.1029/2019JF005201>

- Ikeda, S. (1982). Incipient motion of sand particles on side slopes. *Journal of the Hydraulics Division*, 108(1), 95–114. <https://doi.org/10.1061/JYCEAJ.0005812>
- Iwantoro, A. P., van der Vegt, M., & Kleinhans, M. G. (2020). Morphological evolution of bifurcations in tide-influenced deltas. *Earth Surface Dynamics*, 8(2), 413–429. <https://doi.org/10.5194/esurf-8-413-2020>
- Iwantoro, A. P., van der Vegt, M., & Kleinhans, M. G. (2021). Effects of sediment grain size and channel slope on the stability of river bifurcations. *Earth Surface Processes and Landforms*, 46(10), 2004–2018. <https://doi.org/10.1002/esp.5141>
- Iwantoro, A. P., van der Vegt, M., & Kleinhans, M. G. (2022). Stability and asymmetry of tide-influenced river bifurcations. *Journal of Geophysical Research: Earth Surface*, 127(6), e2021JF006282. <https://doi.org/10.1029/2021JF006282>
- Jansen, P. P., Van Bendegom, L., Van den Berg, J., De Vries, M., & Zanen, A. (1979). *Principles of river engineering: The non-tidal alluvial river*. Pitman.
- Jerolmack, D. J. (2009). Conceptual framework for assessing the response of delta channel networks to Holocene sea level rise. *Quaternary Science Reviews*, 28(17), 1786–1800. <https://doi.org/10.1016/j.quascirev.2009.02.015>
- Jeuken, M. C. J. L., & Wang, Z. B. (2010). Impact of dredging and dumping on the stability of ebb-flood channel systems. *Coastal Engineering*, 57(6), 553–566. <https://doi.org/10.1016/j.coastaleng.2009.12.004>
- Ke, W. T., Shaw, J. B., Mahon, R. C., & Cathcart, C. A. (2019). Distributary channel networks as moving boundaries: Causes and morphodynamic effects. *Journal of Geophysical Research: Earth Surface*, 124(7), 1878–1898. <https://doi.org/10.1029/2019JF005084>
- Kleinhans, M. G., de Haas, T., Lavooi, E., & Makaske, B. (2012). Evaluating competing hypotheses for the origin and dynamics of river anastomosis. *Earth Surface Processes and Landforms*, 37(12), 1337–1351. <https://doi.org/10.1002/esp.3282>
- Kleinhans, M. G., Ferguson, R. I., Lane, S. N., & Hardy, R. J. (2013). Splitting rivers at their seams: Bifurcations and avulsion. *Earth Surface Processes and Landforms*, 38(1), 47–61. <https://doi.org/10.1002/esp.3268>
- Kleinhans, M. G., Jagers, H. R. A., Mosselman, E., & Sloff, C. J. (2008). Bifurcation dynamics and avulsion duration in meandering rivers by one-dimensional and three-dimensional models. *Water Resources Research*, 44(8). <https://doi.org/10.1029/2007WR005912>
- Kleinhans, M. G., & van den Berg, J. H. (2011). River channel and bar patterns explained and predicted by an empirical and a physics-based method. *Earth Surface Processes and Landforms*, 36(6), 721–738. <https://doi.org/10.1002/esp.2090>
- Konkol, A., Schwenk, J., Katifori, E., & Shaw, J. B. (2022). Interplay of river and tidal forcings promotes loops in coastal channel networks. *Geophysical Research Letters*, 49(10), e2022GL098284. <https://doi.org/10.1029/2022GL098284>
- Le, T. B., Crosato, A., Mosselman, E., & Uijtewaald, W. S. J. (2018). On the stability of river bifurcations created by longitudinal training walls. Numerical investigation. *Advances in Water Resources*, 113, 112–125. <https://doi.org/10.1016/j.advwatres.2018.01.012>
- Lee, H. Y., Fu, D. T., & Song, M. H. (1993). Migration of rectangular mining pit composed of uniform sediments. *Journal of Hydraulic Engineering*, 119(1), 64–80. [https://doi.org/10.1061/\(ASCE\)0733-9429\(1993\)119:1\(64\)](https://doi.org/10.1061/(ASCE)0733-9429(1993)119:1(64))
- Lesser, G. R., Roelvink, J. A., van Kester, J. A. T. M., & Stelling, G. S. (2004). Development and validation of a three-dimensional morphological model. *Coastal Engineering*, 51(8–9), 883–915. <https://doi.org/10.1016/j.coastaleng.2004.07.014>
- Luo, X.-L., Zeng, E. Y., Ji, R.-Y., & Wang, C.-P. (2007). Effects of in-channel sand excavation on the hydrology of the Pearl River Delta, China. *Journal of Hydrology*, 343(3), 230–239. <https://doi.org/10.1016/j.jhydrol.2007.06.019>
- Mackin, H. J. (1948). Concept of the graded river. *GSA Bulletin*, 59(5), 463–512. [https://doi.org/10.1130/0016-7606\(1948\)59\[463:cotgr\]2.0.co;2](https://doi.org/10.1130/0016-7606(1948)59[463:cotgr]2.0.co;2)
- Passalacqua, P. (2017). The delta connectome: A network-based framework for studying connectivity in river deltas. *Geomorphology*, 277, 50–62. <https://doi.org/10.1016/j.geomorph.2016.04.001>
- Passalacqua, P., Giosan, L., Goodbred, S., & Overeem, I. (2021). Stable ≠ Sustainable: Delta dynamics versus the human need for stability. *Earth's Future*, 9(7). <https://doi.org/10.1029/2021EF002121>
- Passalacqua, P., & Moodie, A. J. (2022). Delta-scale solutions for human-scale needs. *Science*, 376(6596), 916–917. <https://doi.org/10.1126/science.abq1166>
- Proust, S., Bousmar, D., Riviere, N., Paquier, A., & Zech, Y. (2009). Nonuniform flow in compound channel: A 1-D method for assessing water level and discharge distribution. *Water Resources Research*, 45(12). <https://doi.org/10.1029/2009WR008202>
- Qiu, J., Liu, B., Yang, F., Wang, X., & He, X. (2022). Quantitative stress test of compound coastal-fluvial floods in China's Pearl River Delta. *Earth's Future*, 10(5), e2021EF002638. <https://doi.org/10.1029/2021EF002638>
- Ragno, N., Redolfi, M., & Tubino, M. (2021). Coupled morphodynamics of river bifurcations and confluences. *Water Resources Research*, 57(1), e2020WR028515. <https://doi.org/10.1029/2020WR028515>
- Ragno, N., Tambroli, N., & Pittaluga, M. B. (2022). Competing feedback in an idealized tide-influenced delta network. *Environmental Fluid Mechanics*, 22(2–3), 535–557. <https://doi.org/10.1007/s10652-022-09857-2>
- Redolfi, M., Zolezzi, G., & Tubino, M. (2019). Free and forced morphodynamics of river bifurcations. *Earth Surface Processes and Landforms*, 44(4), 973–987. <https://doi.org/10.1002/esp.4561>
- Riquier, J., Piégay, H., Lamouroux, N., & Vaudor, L. (2017). Are restored side channels sustainable aquatic habitat features? Predicting the potential persistence of side channels as aquatic habitats based on their fine sedimentation dynamics. *Geomorphology*, 295, 507–528. <https://doi.org/10.1016/j.geomorph.2017.08.001>
- Salter, G., Paola, C., & Voller, V. R. (2018). Control of delta avulsion by downstream sediment sinks. *Journal of Geophysical Research: Earth Surface*, 123(1), 142–166. <https://doi.org/10.1002/2017JF004350>
- Salter, G., Voller, V. R., & Paola, C. (2020). Chaos in a simple model of a delta network. *Proceedings of the National Academy of Sciences of the United States of America*, 117(44), 27179–27187. <https://doi.org/10.1073/pnas.2010416117>
- Shaw, J. B., Mason, K. G., Ma, H., & McCain, G. W., III. (2021). Influences on discharge partitioning on a large river delta: Case study of the Mississippi-Atchafalaya diversion, 1926–1950. *Water Resources Research*, 57(5), e2020WR028090. <https://doi.org/10.1029/2020WR028090>
- Slingerland, R., & Smith, N. D. (1998). Necessary conditions for a meandering-river avulsion. *Geology*, 26(5), 435–438. [https://doi.org/10.1130/0091-7613\(1998\)026<0435:NCFAMR>2.3.CO;2](https://doi.org/10.1130/0091-7613(1998)026<0435:NCFAMR>2.3.CO;2)
- Syvitski, J. P. M., Kettner, A. J., Correggiari, A., & Nelson, B. W. (2005). Distributary channels and their impact on sediment dispersal. *Marine Geology*, 222–223, 75–94. <https://doi.org/10.1016/j.margeo.2005.06.030>
- Syvitski, J. P. M., & Saito, Y. (2007). Morphodynamics of deltas under the influence of humans. *Global and Planetary Change*, 57(3–4), 261–282. <https://doi.org/10.1016/j.gloplacha.2006.12.001>
- van Denderen, R. P., Schielen, R. M. J., Blom, A., Hulscher, S. J. M. H., & Kleinhans, M. G. (2018). Morphodynamic assessment of side channel systems using a simple one-dimensional bifurcation model and a comparison with aerial images. *Earth Surface Processes and Landforms*, 43(6), 1169–1182. <https://doi.org/10.1002/esp.4267>
- van Dijk, W. M., Schuurman, F., van de Lageweg, W. I., & Kleinhans, M. G. (2014). Bifurcation instability and chute cutoff development in meandering gravel-bed rivers. *Geomorphology*, 213, 277–291. <https://doi.org/10.1016/j.geomorph.2014.01.018>

- van Maren, D. S., Beemster, J. G. W., Wang, Z. B., Khan, Z. H., Schrijvershof, R. A., & Hoitink, A. J. F. (2023). Tidal amplification and river capture in response to land reclamation in the Ganges-Brahmaputra delta. *Catena*, 220, 106651. <https://doi.org/10.1016/j.catena.2022.106651>
- Wang, J., Dijkstra, Y. M., & de Swart, H. E. (2022). Mechanisms controlling the distribution of net water transport in estuarine networks. *Journal of Geophysical Research: Oceans*, 127(1), e2021JC017982. <https://doi.org/10.1029/2021JC017982>
- Wang, Y., Zhou, L., Wan, X., Liu, X., Wang, W., & Yi, J. (2023). Study on sedimentary evolution of the Hanjiang River delta during the late quaternary. *Applied Sciences*, 13(7), 4579. <https://doi.org/10.3390/app13074579>
- Wang, Y.-H., Cai, S.-L., Yang, Y.-D., Zhong, Z.-Y., & Liu, F. (2021). Morphological consequences of upstream water and sediment changes and estuarine engineering activities in Pearl River Estuary channels over the last 50 years. *Science of the Total Environment*, 765, 144172. <https://doi.org/10.1016/j.scitotenv.2020.144172>
- Wang, Z. B., De Vries, M., Fokkink, R. J., & Langerak, A. (1995). Stability of river bifurcations in 1D morphodynamic models. *Journal of Hydraulic Research*, 33(6), 739–750. <https://doi.org/10.1080/00221689509498549>
- Wang, Z. B., Van Maren, D. S., Ding, P. X., Yang, S. L., Van Prooijen, B. C., De Vet, P. L. M., et al. (2015). Human impacts on morphodynamic thresholds in estuarine systems. *Continental Shelf Research*, 111, 174–183. <https://doi.org/10.1016/j.csr.2015.08.009>
- Wang, Z. B., Wang, Z. Y., & de Vriend, H. J. (2008). Impact of water diversion on the morphological development of the Lower Yellow River. *International Journal of Sediment Research*, 23(1), 13–27. [https://doi.org/10.1016/S1001-6279\(08\)60002-5](https://doi.org/10.1016/S1001-6279(08)60002-5)
- Wohl, E., Bledsoe, B. P., Jacobson, R. B., Poff, N. L., Rathburn, S. L., Walters, D. M., & Wilcox, A. C. (2015). The natural sediment regime in rivers: Broadening the foundation for ecosystem management. *BioScience*, 65(4), 358–371. <https://doi.org/10.1093/biosci/biv002>
- Wu, B., Zheng, S., & Thorne, C. R. (2012). A general framework for using the rate law to simulate morphological response to disturbance in the fluvial system. *Progress in Physical Geography*, 36(5), 575–597. <https://doi.org/10.1177/0309133312436569>
- Ylla Arbós, C., Blom, A., Sloff, C. J., & Schielen, R. M. J. (2023). Centennial channel response to climate change in an engineered river. *Geophysical Research Letters*, 50(8), e2023GL103000. <https://doi.org/10.1029/2023GL103000>
- Yuill, B. T., Gaweesh, A., Allison, M. A., & Meselhe, E. A. (2016). Morphodynamic evolution of a lower Mississippi River channel bar after sand mining. *Earth Surface Processes and Landforms*, 41(4), 526–542. <https://doi.org/10.1002/esp.3846>
- Zheng, S., Wang, H., & Wu, B. (2022). Delayed morphological adjustment of the Yellow and lower Wei Rivers upstream of the Sanmenxia dam at multi-temporal scales. *Catena*, 212, 106035. <https://doi.org/10.1016/j.catena.2022.106035>